31st EUROPEAN ROTORCRAFT FORUM

Session Aerodynamics
Paper #84

INDUSTRIAL VALIDATION OF CFD SOLVERS ON MEDIUM AND LARGE HELICOPTER FUSELAGES

Progress through advanced turbulence models applied to separated flows

by

A. D´Alascio*, C. Castellin**, B. Schöning[♦]

*EUROCOPTER DEUTSCHLAND GmbH, München, Germany

**EUROCOPTER S.a.S, Marignane France

[♦]DLR, Deutsches Zentrum für Luft und Raumfahrt e.V. in der Helmholtz-Gemeinschaft, Braunschweig, Germany

SEPTEMBER 13 - 15, 2005
FLORENCE
ITALY

Industrial validation of CFD solvers on medium and large helicopter fuselages

Progress through advanced turbulence models applied to separated flows

A. D´Alascio[*], C. Castellin[**], B. Schöning[♦]

[*] Eurocopter Deutschland GmbH, Munich, Germany
[**] Eurocopter S.a.S, Marignane, France
[♦] DLR, Deutsches Zentrum für Luft und Raumfahrt e.V. in der Helmholtz-Gemeinschaft, Braunschweig, Germany

Abstract

The paper deals with the validation of three different CFD solvers, in use at EUROCOPTER, on two industrial test cases: a medium and a large helicopter fuselage. The validation activity is being carried out within the Franco-German bi-national research project CHANCE [1], [2]. After a brief description of the three RANS flow solvers, the validation activity results have been reported. The validation results have been structured in two main parts. The first part presents a comparison between the CFD results and the wind tunnel measurements about the isolated fuselage of the EC145 medium weight helicopter fuselage in level flight conditions at medium flight speed. The multi-block structured RANS code FLOWer and the unstructured RANS code TAU developed by DLR have been used for this analysis. This section documents the continuation with respect to the validation activity already presented in [10]. The second part of the paper presents a shape effect analysis on all aerodynamic coefficients of the isolated fuselage of a large transport helicopter. The effect of the engine cowling has been computed by CFD and compared with existing wind tunnel data. This study has been carried out by applying the elsA multi-block structured RANS flow solver developed by ONERA.

Nomenclature

Symbols

C_d	Drag coefficient. $= D/(q_\infty S_{ref})$
C_l	Lift coefficient $= L/(q_\infty S_{ref})$
C_X	Longitudinal force coefficient $= F_X/(q_\infty S_{ref})$
C_Y	Side force coefficient $= F_Y/(q_\infty S_{ref})$
C_Z	Vertical force coefficient $= F_Z/(q_\infty S_{ref})$
C_L	Roll moment coefficient $= M_X/(q_\infty S_{ref} \cdot L_{ref})$
C_M	Pitch moment coefficient $= M_Y/(q_\infty S_{ref} \cdot L_{ref})$
C_N	Yaw moment coefficient $= M_Z/(q_\infty S_{ref} \cdot L_{ref})$
D	Drag force [N]
L	Lift force [N]
L_{ref}	Reference length
M	Moment
M_∞	Free stream Mach number
P	Pressure
q_∞	Dynamic pressure $= 1/2\rho_\infty v_\infty^2$
Re	Reynolds number
S_{ref}	Reference surface
TPL	Total Pressure Losses $= 1 - P_{TOT}/P_{TOT\infty}$
u,v,w	Cartesian velocity components
X,Y, Z	Cartesian co-ordinates X pointing in nose-tail direction Y pointing in left-right direction Z pointing in vertical direct., bottom-up
y^+	$= \rho_{wall} u_t y/\mu_{wall}$ being u_t the local tangential velocity and y the vertical direction
α	Angle of attack
β	Side slip angle
μ	Dynamic viscosity
ρ	Air density

Acronyms

CAD	Computer Aided Design
CFD	Computational Fluid Dynamics
LEA	Linear Explicit Algebraic stress model
PIV	Particle Image Velocimetry
RANS	Reynolds-Averaged Navier-Stokes
RSM	Reynolds Stress Model
SST	Shear Stress Tensor

Introduction

Helicopter fuselages are not always smooth streamlined bodies like airplanes usually are. The ability to hover makes the helicopter the ideal machine for rescue missions, surveillance, transport of people and goods to uneasily reachable locations, *e.g.* oil-extraction platforms, mountains, etc. It is often required that the helicopter fuselage be a blunt body. A backdoor, for instance, necessary to easily and quickly load injured people into a rescue machine requires that the back of the fuselage has a steep junction with the tail boom. In order to optimise these peculiar shapes, aerodynamic simulation tools are required, which provide reliable results also when flow separation occurs. Unsteady RANS equations have reached a high degree of accuracy for moderate detached flows. A polar curve of a wing can be quite accurately computed till stall conditions. When massive separation occurs, the classical 2-equations turbulence models fail and unsteady turbulence models such as DES or LES are required. The objective of this paper is to investigate the effect of the most advanced RANS turbulence models, such as the 2-equation SST model by Menter, the Reynolds Stress Model and others, on particularly complex helicopter fuselages, such as the EC145 depicted in Figure 1-*left* and the NH90 presented in Figure 1-*right*.

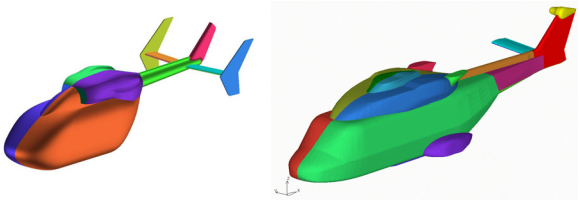

EC145 **NH90**

Figure 1: Medium (EC145) and large (NH90) helicopter fuselages

The RANS flow solvers

The multi-block structured code elsA

The elsA solver [3] is a multi-application object oriented aerodynamic code of which the development started at ONERA in 1997. It is based on a cell-centred finite volume technique for structured multi-block meshes and includes a wide range of numerical techniques as well as physical models in order to simulate the flowfield around realistic aerospace configurations from the low subsonic to the hypersonic regime. The domain of application includes fixed wing, rotary wing, turbo-machinery, space launcher and missile configurations. In the present activity, the spatial discretisation used is the standard Jameson's second-order centred scheme with explicit artificial viscosity terms using second and fourth differences. For the time integration an explicit 4-stage Runge-Kutta algorithm, together with implicit residual smoothing is applied. For steady-state problems, local time-stepping and multigrid acceleration techniques are applied to speed-up convergence. Low-Mach number preconditioning technique is also available for very low speed flows. For unsteady applications, either the dual-time stepping technique or the Gear time-integration scheme is generally used for an implicit formulation of the problem. The former allows using all the techniques developed for steady-state solutions during the internal sub-iterations, while the latter uses Newton sub-iterations at each time step to reach convergence. The implicit system is solved using LU decomposition.

The multi-block structured code FLOWer

The FLOWer flow solver [4], [5] is the Navier-Stokes code developed by DLR, which is being enhanced for rotorcraft applications within the frame of the Franco-German CHANCE [1], [2] research project supported on the German side by the Ministry of Economics. It solves the compressible, three-dimensional unsteady Reynolds-averaged Navier-Stokes equations on block structured meshes around bodies in arbitrary motion. FLOWer implements two different spatial discretisation schemes, based on finite volume formulation, where the flow variables are located either at the vertices or at the cell centres.
The baseline method employs a central space discretisation with artificial viscosity and an explicit five stage Runge-Kutta time integration scheme. Local time-stepping, implicit residual smoothing and multigrid are used to accelerate convergence. Turbulence is modelled by algebraic or by advanced transport equation models, *e.g.* the 2-equation k-ω model or the 7-equation Reynolds Stress Model [8], [9]. Low velocity preconditioning, deforming meshes and the Chimera technique are also available.

The unstructured code TAU

The main developments for the unstructured Navier-Stokes code TAU of DLR were based on the national CFD project MEGAFLOW [6] within the framework of the German aerospace program, which combined activities from DLR, German universities and aircraft industry. Other national, bi-national and European co-operations have contributed to the development and maturity of the TAU code [7].

The TAU code is an unstructured method based on a dual mesh approach, which is well suited for hybrid grids thus allowing the use of mixed-element meshes composed of tetrahedrons, prisms, hexahedrons, and/or pyramids. The combination of these elements is considered to allow for regular grids in the vicinity of walls (high boundary layer resolution) in the combination with the more flexible tetrahedral elements in the remaining computational domain. The dual grid is stored in an edge based data structure, which makes the solver independent of the element types of the primary grid. In order to employ a multigrid technique the agglomeration approach is used to obtain coarse grids by fusing together the fine grid control volumes. For turbulent flows different 1- and 2-equation turbulence models are implemented.
The integration in time is done employing an explicit Runge-Kutta time stepping algorithm, which, as part of a dual time stepping approach, can also be applied to transient flows. In order to efficiently resolve detailed flow features, a grid adaptation algorithm for hybrid meshes based on local grid refinement is available.
Specific features of the TAU-Code are the grid adaptation capability and the effective use of parallel computers.

The EC145 helicopter fuselage

This chapter presents the results of the comparison between the structured code FLOWer and the unstructured code TAU, and the experimental data measured during the wind tunnel campaign carried out at EUROCOPTER Marignane (France) in 1997 on the BK117-C2 helicopter model. During the wind tunnel campaign, all global values, *i.e.* lift, drag, side force and the three pitch, roll and yaw moments were recorded at different angles of attack α and side slip angles β. Unfortunately at that time it was neither decided to instrument the fuselage model with pressure taps nor to perform PIV measurements in the field. Therefore the comparison in terms of local quantities on the fuselage surface and in the field has been made only between different prediction results obtained with the FLOWer and TAU flow solvers using different turbulence models.
The EC145 fuselage shape is almost identical to the BK117-C2 model one. As shown in Figure 2, the two surface geometries, the EC145 in colour and the BK117-C2 in grey, differ basically in three regions: the conical junction between the two air inlets and the fuselage cabin roof, the fuselage back and the horizontal stabilisers and endplates. The engine cowling, tail boom, vertical fin and the rest of the fuselage are identical. The most significant differences can be indeed identified in the position and width of the horizontal stabilisers, in the shape and surface extension of the endplates. As a consequence the contribution to the loads of these lifting surfaces has been subtracted from the wind tunnel measurements and from the CFD computation, *i.e.* the CFD model contains the horizontal stabiliser and endplate but the loads integration on these surfaces has been excluded in the post processing phase. It is obvious that the difference in the shape of the fuselage back, Figure 2, will have a considerable effect on the separation zone when comparing the flow around the BK117-C2 and the EC145 geometry.
The chapter has been divided in three sections. The first deals with the mesh generation for both the structured and the unstructured solver, the second describes in detail the analysis of the CFD results and the third reports the future activity related to the CFD validation on the EC145 helicopter fuselage.

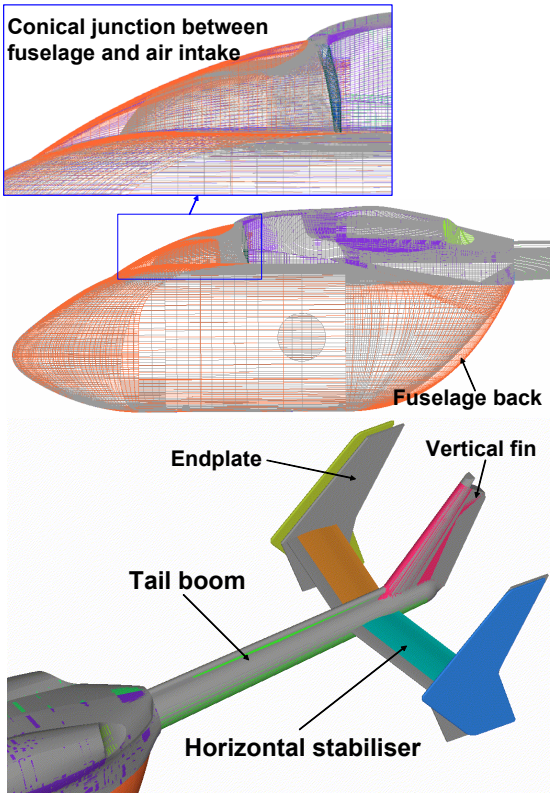

Figure 2: Comparison between the EC145 helicopter fuselage in colour and the BK117-C2 wind tunnel model in grey.

Mesh generation

The surface grid generation started from the CATIA v.4 surface mesh of the EC145 helicop-

ter already available in the design department. The structural CAD model has been cleaned and simplified by completely removing main and tail rotor, landing gear, antennas and handles. The air intakes and jet exhausts have been closed and all gaps between adjacent surface patches have been repaired. Figure 1-left shows the aerodynamic “water tight” CATIA model obtained after the above mentioned activity. The same CAD surface model has been used to generate the multi-block structured volume grid for the FLOWer code and the unstructured hybrid one for the TAU code.

The structured multi-block Navier-Stokes mesh was generated by applying the grid generator ICEM-Hexa [11]. The resulting mesh around the isolated fuselage is composed of 64 blocks, 4.9 million nodes and allows 3 levels of multigrid. The topology structure is a C-O, with the C-structure in the longitudinal direction and the O-structure in the transversal one. A boundary layer grid has also been generated around the whole surfaces. Figure 3 shows the middle coordinate grid plane. The C-topology structure in the grid longitudinal direction is visible here. Figure 4 shows two transversal coordinate planes through the engine cowling (left) and the stabilisers (right). The O-topology structure in the grid transversal direction can be identified.

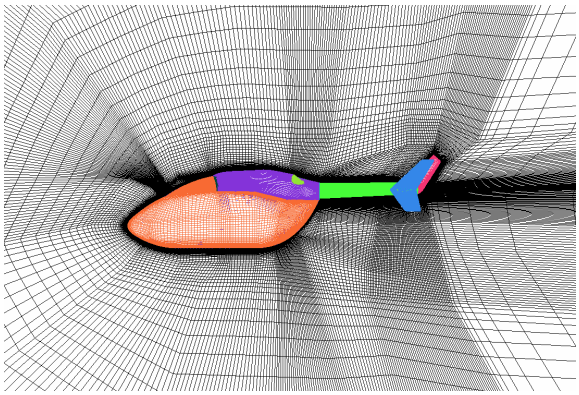

Figure 3: ICEM-Hexa structured multi-block N.-S. mesh around the EC145 isolated fuselage: middle plane.

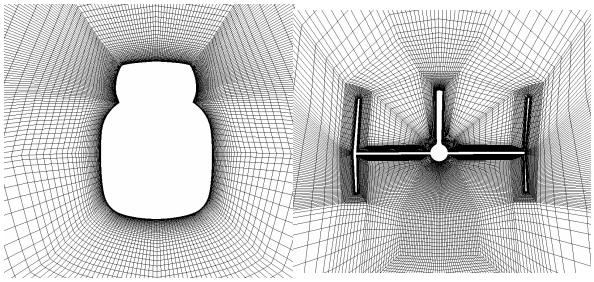

Figure 4: ICEM-Hexa structured multi-block N.-S. mesh around the EC145 isolated fuselage: transversal plane through the engine cowling (left) and stabilisers (right).

The CENTAUR software [12] was used to generate the hybrid unstructured Navier-Stokes mesh around the EC145 helicopter fuselage. The starting hybrid mesh is composed of 3.7 million nodes; it has 25 prism layers around the surface discretised by 88715 points. Figure 4 shows a cut through the fuselage middle plane, whereas Figure 6 shows a transversal cut through the fuselage engine cowling.

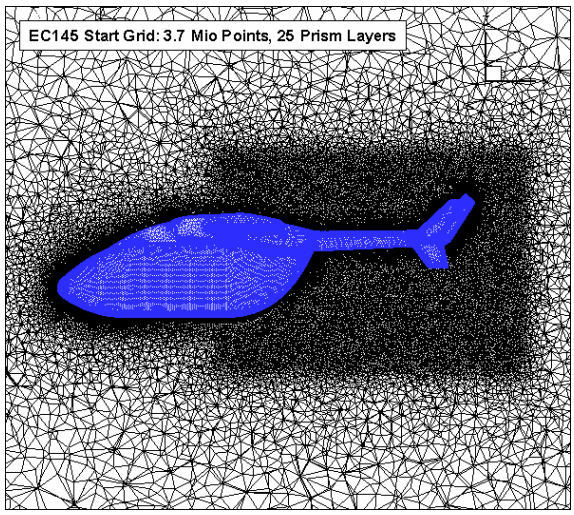

Figure 5: CENTAUR hybrid N.-S. starting mesh around the EC145 isolated fuselage: middle plane.

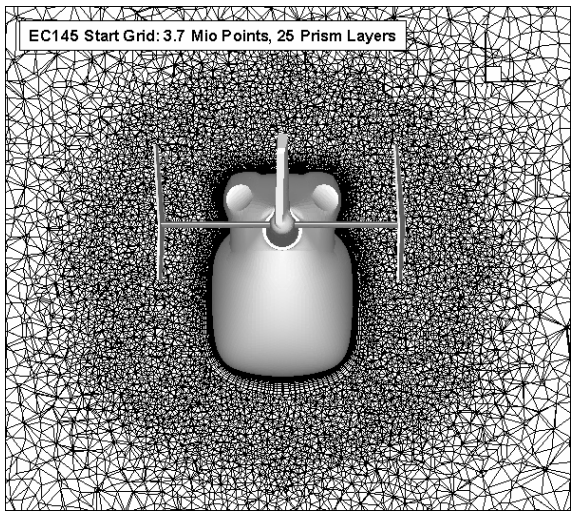

Figure 6: CENTAUR hybrid N.-S. starting mesh around the EC145 isolated fuselage: transversal plane through the engine cowling.

During run the TAU code offers the possibility of adapting the hybrid mesh according to a scalar quantity computed in the field around the fuselage. Using the Total Pressure Losses field as the driving scalar quantity, 2 mesh adaptation cycles were made in order to better capture the vorticity field behind the fuselage. The final

adapted mesh, depicted in Figure 7, is composed of 5.3 million nodes. The 25 prism layers were not modified. The mesh adaptation had the objective of refining the mesh in the wake region behind the fuselage and the empennages.

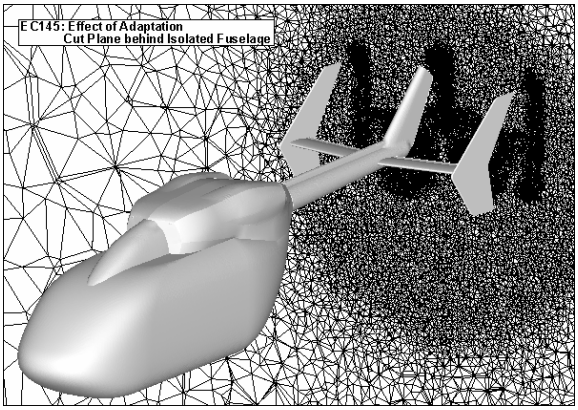

Figure 7: CENTAUR hybrid N.-S. final adapted mesh around the EC145 isolated fuselage: transversal plane downstream of the tail unit.

The y^+ calculated on the body surfaces for both FLOWer and TAU code have a maximum value of 1.0, therefore the grid is fine enough to capture the strong gradients occurring in the boundary layer.

Analysis of results

The section presents the comparison between the FLOWer and TAU prediction results, and the wind tunnel measurements in terms of global loads. As no local quantities were measured during the BK117-C2 1997 wind tunnel campaign, the comparison in terms of scalar quantities on the fuselage surface and in the field have been done only between the different numerical results.
Two FLOWer runs for each fuselage attitude α (α= -18º, -12º, -6º, 0º, 6º, 12º) have been done, the first by using the 2-equation k-ω turbulence model applying the SST correction by Menter and the second by using the 7-equation RSM SSG/LRR-ω turbulence implementing the simple gradient diffusion model [8], [9]. All other control parameters have been kept constant. Two TAU runs for each fuselage attitude α (α= -12º, -6º, 0º, 6º) have been made, the first by using the 2-equation standard Wilcox k-ω turbulence model and the second the k-ω turbulence model but applying the SST correction by Menter. All other control parameters have been kept constant. In all computations the side slip angle was β=0º.

Figure 8 shows the comparison between the FLOWer and TAU results and the wind tunnel measurements in terms of drag *(top),* lift *(middle)* and pitching moment coefficient *(bottom)* versus fuselage angle of attack α. The incidence angle is negative for a fuselage nose down attitude. The contribution to the forces and moment of the horizontal stabilisers and endplates has been subtracted, in a post processing phase, from both wind tunnel measurements and CFD results. In fact the differences in the shape of these components, as shown in Figure 2, are expected to produce considerable differences in the global forces and even more in the moments.

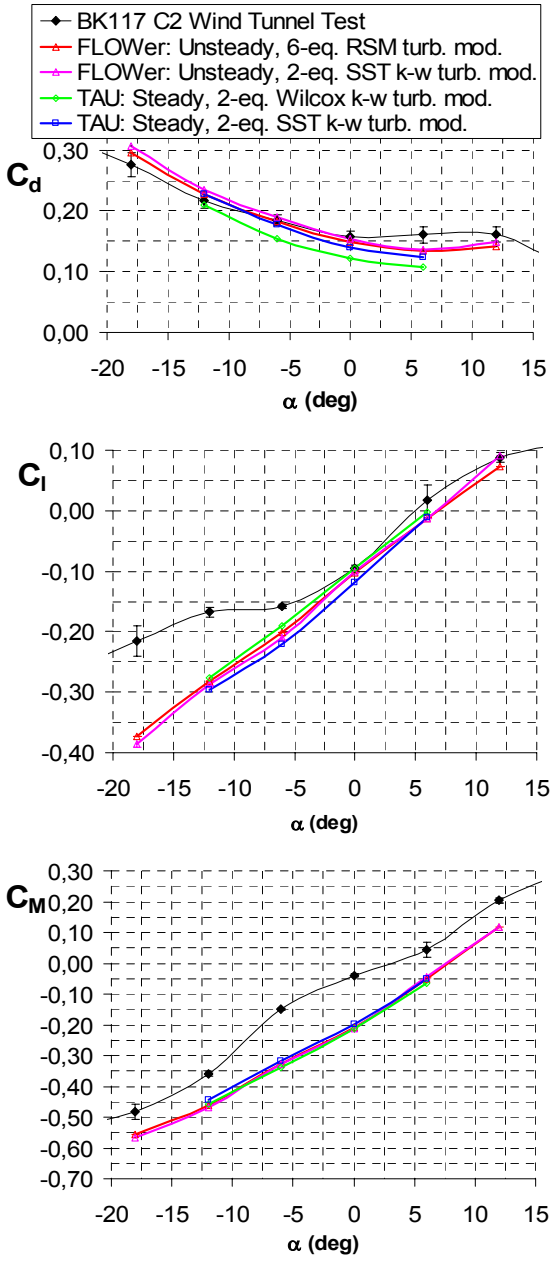

Figure 8: Drag *(top),* Lift *(middle)* and Pitching moment *(bottom)* coefficient versus fuselage angle of attack α=0°

The **drag** figure predicted by both FLOWer runs and by the TAU one applying the SST k-ω turbulence model correlate very well with the wind tunnel measurements especially in the range of α comprised between -12° and 0° which is the operational region for the fuselage in forward flight conditions. The TAU results, applying the standard Wilcox k-ω model, slightly underestimate the drag figure.
In the range of α comprised between -6° and 12° all codes predict the **lift** figure satisfactorily. The highest discrepancy between computations and measurements occurs below α=–6°. In this region the wind tunnel data show an unusual non linear trend which contradicts previous wind tunnel campaigns carried out on different helicopters but with similar blunt fuselages. In previous campaigns, in fact, the lift curve did not present any curvature change in the range considered in this study. Therefore, even though a definite conclusion cannot be drawn, all CFD results might be reliable (see also [10]).
Looking at the **pitching moment** figure, all CFD results are in a perfect agreement among themselves, but they show a constant underestimation with respect to the wind tunnel measurements. Furthermore none of the CFD results presents the flex around α=-6°. Unfortunately the uncertainties related to the wind tunnel measurements and the discrepancies between the EC145 helicopter fuselage and the BK117-C2 wind tunnel model shape do not allow drawing a final conclusion. Nevertheless the fact that the FLOWer and the TAU codes applied on different grids, by using different turbulence models, present almost identical results highlights the necessity of a deeper experimental investigation of this test case.

Figure 9 and Figure 10 show the pressure coefficient distribution on the EC145 helicopter fuselage obtained at α=0° respectively by the FLOWer flow solver, using the SST k-ω (Figure 9-*top*) and the RSM (Figure 9-*bottom*) turbulence models, and by the TAU code, using the standard Wilcox k-ω (Figure 10-*top*) and the SST k-ω (Figure 10-*bottom*) turbulence models. All four prediction results appear to be almost identical on the fuselage cabin and on the engine cowling. Some differences can be seen on the tail boom and on the horizontal stabilisers and vertical fin. Here the flow is strongly influenced by the wake, which detaches from the fuselage back region and, convected downstream, interacts with the helicopter tail.

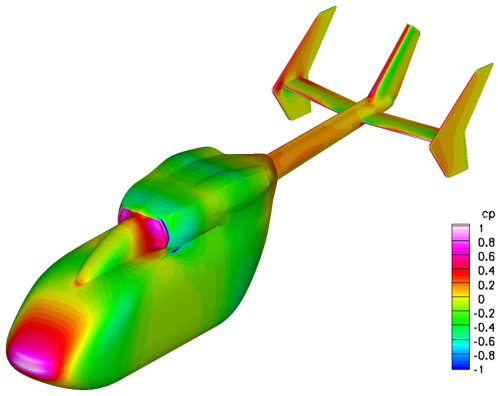

2-equation SST k-ω turbulence model

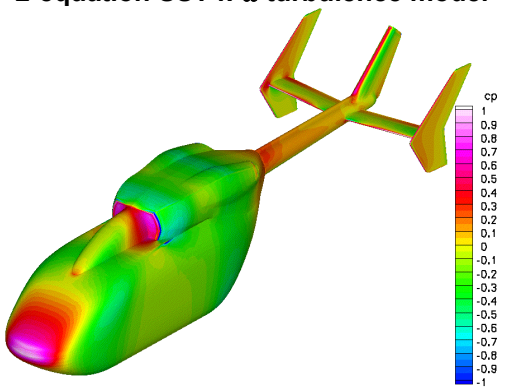

7-equation RSM turbulence model

Figure 9: **FLOWer** results for α=0°: Cp distribution on the EC145 isolated fuselage.

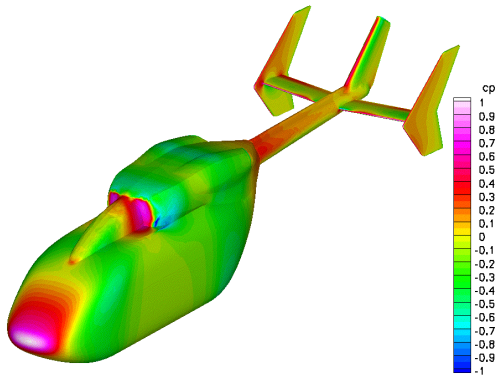

2-equation Wilcox k-ω turbulence model

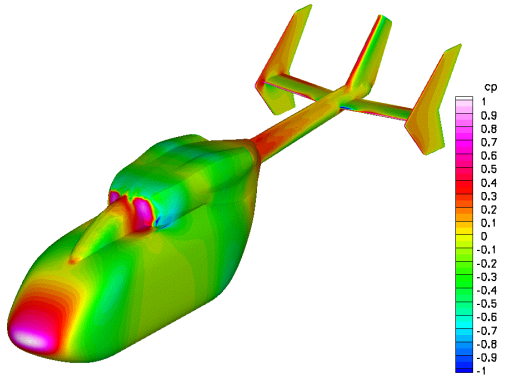

2-equation SST k-ω turbulence model

Figure 10: **TAU** results for α=0°: Cp distribution on the EC145 isolated fuselage.

The skin friction lines over-imposed to the pressure coefficient distribution in the separation region on the fuselage backdoor is shown in the following Figure 11, as computed by FLOWer, and in Figure 12, as computed by TAU. Once again each figure shows the solutions relative to the two different turbulence models used. All CFD computations predict a large flow separation covering almost the entire backdoor area. The extension of the separation region is quite similar in all CFD computations. The skin friction patterns are different showing slightly different positions of the two vortices which detach from the fuselage backdoor.

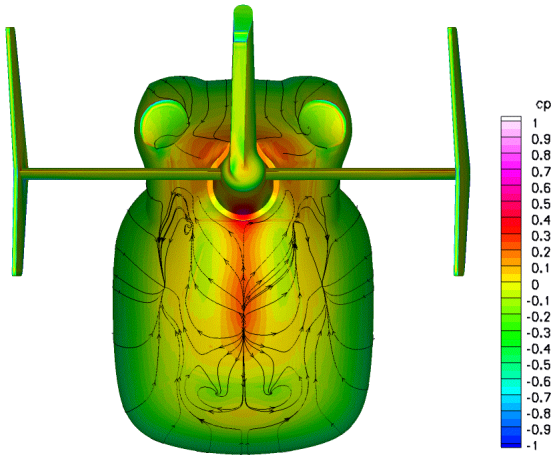

2-equation SST k-ω turbulence model

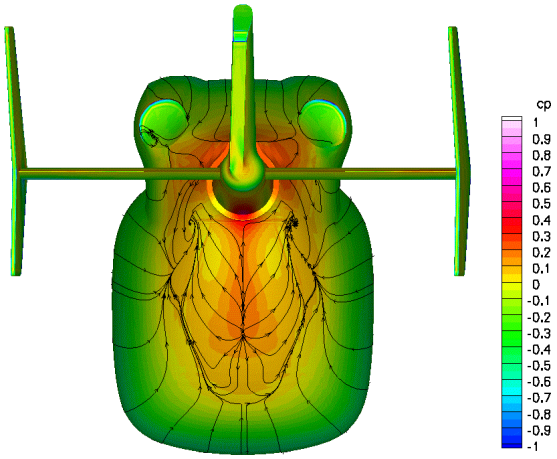

7-equation RSM turbulence model

Figure 11: **FLOWer** results for α=0°: Cp distribution with superimposed friction lines on the EC145 isolated fuselage back door region.

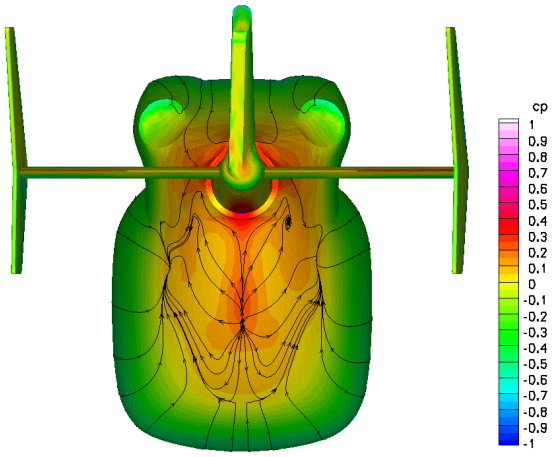

2-equation Wilcox k-ω turbulence model

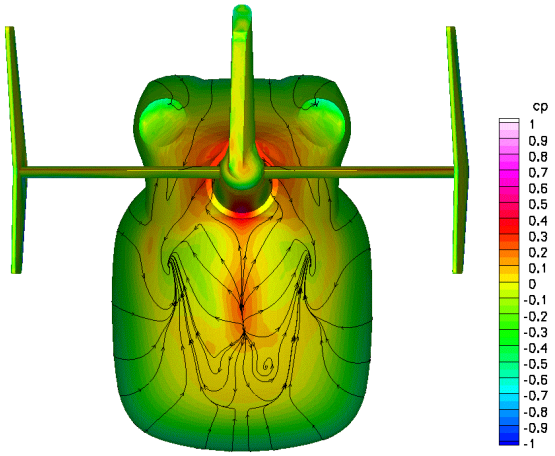

2-equation SST k-ω turbulence model

Figure 12: TAU results for α=0°: Cp distribution with superimposed friction lines on the EC145 isolated fuselage back door region.

Figure 13 and Figure 14 show the Total Pressure Losses TPL on the fuselage mid-plane as computed by FLOWer and TAU respectively for a fuselage attitude of α=0°: Once again all pictures are very similar. By looking at the FLOWer solutions of Figure 13, the SST model appears to be slightly more dissipative with respect to the RSM model in the fuselage wake region. The same can be said comparing the TAU prediction results obtained with the standard Wilcox and the SST k-ω turbulence model of Figure 14. Indeed similar plots of the ratio between the turbulent and laminar eddy viscosity μ_T/μ_L show higher values in the wake region for the k-ω model implementing the SST correction. It is to be noted that the k-ω SST solution with the TAU code shows a more refined wake than the FLOWer solution with the same turbulence model. The reason for this is the local grid adaptation which was performed with TAU and which is not available in a structured code like FLOWer. The refinement region was restricted intentionally to the vicinity of the fuselage in order to limit the computational effort.

This explains the sudden smearing of the wake in Figure 14 at about 15% fuselage length downstream of the tail fin.

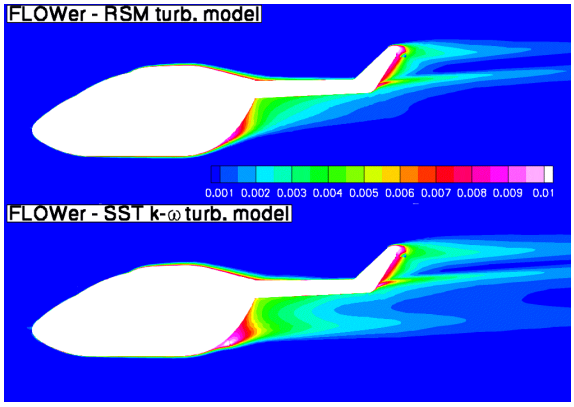

Figure 13: FLOWer results for α=0°: TPL distribution on the fuselage mid-plane of the EC145 helicopter.

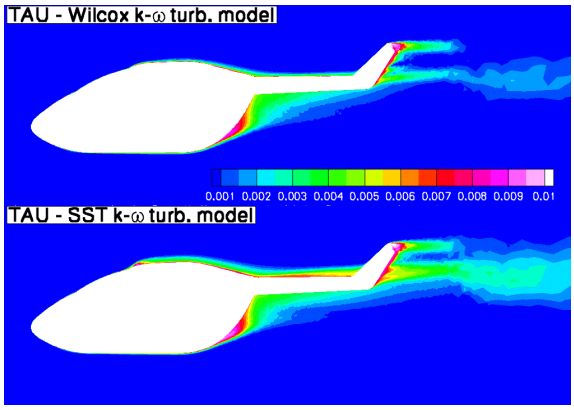

Figure 14: TAU results for α=0°: TPL distribution on the fuselage mid-plane of the EC145 helicopter.

Figure 15, Figure 16 and Figure 17 show the comparison of all CFD results in terms of pressure coefficient distribution respectively on the fuselage midsection Y=0, on the horizontal 2D cut through the fuselage cabin just above its nose at Z=280 [mm] (see Figure 18 for the position of the horizontal cut) and on the midsection of the right horizontal stabiliser. The qualitative good correlation between the CFD results already mentioned by comparing Figure 9 with Figure 10 is quantitatively confirmed here: on the fuselage cabin the four numerical solutions are practically identical (see Figure 15). Some slight differences are encountered on the tail fin, whereas the biggest differences are encountered on the fuselage back door (see Figure 16) and on the horizontal stabilisers (see Figure 17). The differences between the four prediction results on the horizontal stabilisers do not reflect in a discrepancy between the global forces and moments in Figure 8 because, as mentioned before, the contribution of these components has been subtracted from the total values in a post processing phase.

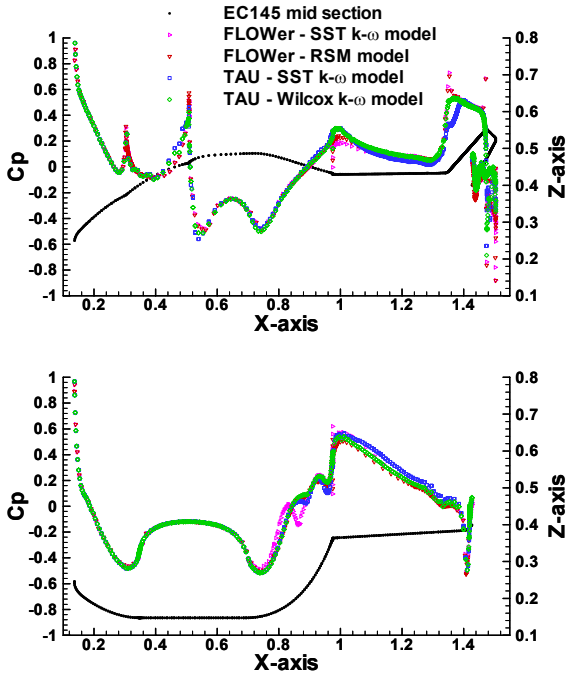

Figure 15: Comparison of results for α=0°: Cp distribution on the mid-section (y=0) of the EC145 isolated fuselage.

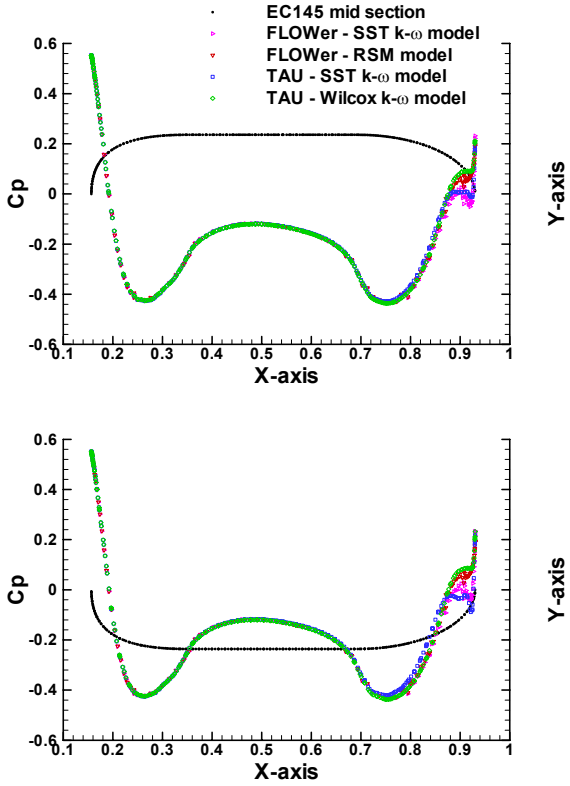

Figure 16: Comparison of results for α=0°: Cp distribution on the horizontal section Z=280[mm] through the EC145 isolated fuselage cabin.

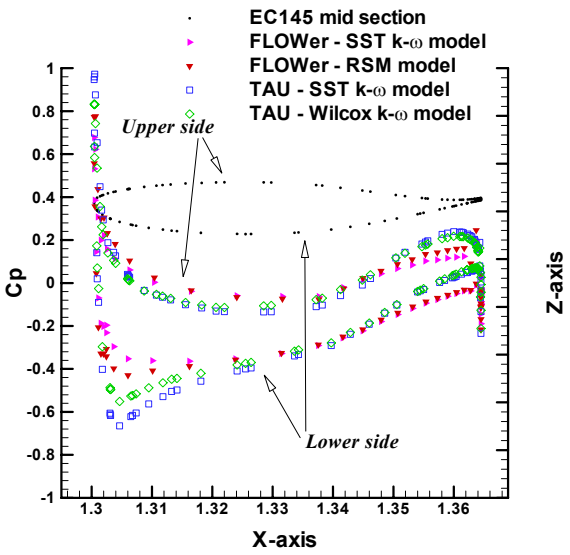

Figure 17: Comparison of results for α=0°: Cp distribution on the mid-section of the right horizontal stabiliser of the EC145 isolated fuselage.

Future activity

In order to answer the questions still open about the EC145 validation activity, EUROCOPTER DEUTSCHLAND decided to perform new wind tunnel measurements on the BK117-C2 model of Figure 18.

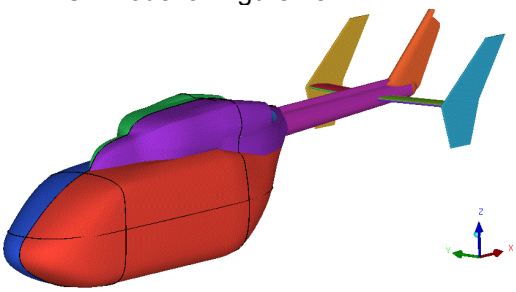

Figure 18: BK117-C2 model to be tested in the Technische Universität München.

The new wind tunnel campaign will be carried out during the 2nd half of 2005 at the Technical University of Munich. Subsequently new meshes will be generated around the BK117-C2 model and new CFD computations will be run. The meshes shall now model also the wind tunnel sting and floor. The model will be instrumented with 83 static pressure ports. Furthermore three PIV windows will be located behind the fuselage in order to visualise the wake shed by the fuselage cabin. Visualisation of the transition region on the fuselage nose and of the separation region on the fuselage backdoor has also been planned. The new data base will be used at ECD to validate the challenging industrial test case in the DESider (Detached Eddy Simulation for industrial aerodynamics) project partly financed by the E.U. within the 6th Framework Program. Here unsteady turbulence models such as DES, LES hybrid RANS-LES and embedded LES will be validated both on simple but very well documented test cases and more complex ones of industrial relevance.

The large transport helicopter fuselage

The section presents the comparison between the elsA code prediction results and some wind tunnel measurements available at EUROCOPTER. The validation test case is the NH90 model measured in the LST wind tunnel of DNW. The contribution of the engine cowling to the drag, lift and side force coefficients has been computed by elsA and compared with the wind tunnel measurements. In order to compute the cowling fairing effect on the isolated fuselage two shapes have been considered: a reference one with smooth fuselage and sponsons (see Figure 19-top) and a second one including also one of the cowling fairings available for the wind tunnel tests (see Figure 19-bottom). The difference between the global loads acting on the two models gives the cowling fairing contribution to the loads. The fuselage shape was simplified by removing the vertical fin and the horizontal stabiliser.

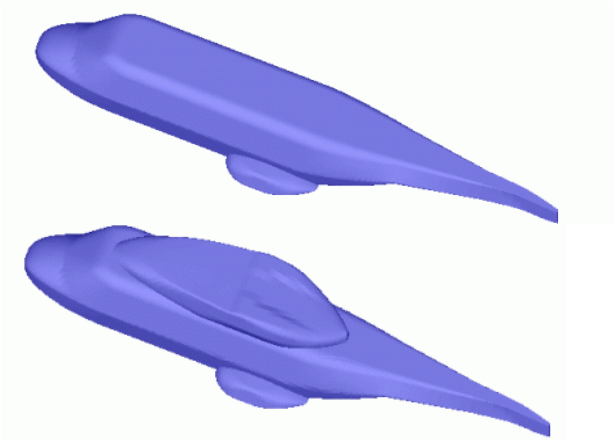

Figure 19: NH90 fuselage model with (bottom) and without (top) the engine cowling.

The Navier-Stokes grid around both helicopter models is composed of one hundred coincident structured blocks and of a total cell number of 2.6 millions. The first cell size on the fuselage wall allows obtaining a y^+ of 0.8, the grid spacing on the proximity of the walls is fine enough to correctly model the boundary layer. The turbulence model used for all RANS computations is the Wilcox 2-equation k-ω model with the SST correction by Menter. Preconditioning was also used to accelerate convergence.

A sweep on the incidence and on the sideslip angle has been performed for angles varying in the range between -6 and +6 degrees. The contribution of the engine cowling to the aerodynamic coefficients as predicted by the elsA code has then been compared with the corresponding measured quantities. The aerodynamic coefficients corresponding to the 6 axis of the wind tunnel balance have been considered for all incidence and sideslip angles. Figure 20 shows the contribution of the cowling fairing to the drag versus incidence angle. Both elsA predictions and wind tunnel measurements have been plot. The uncertainty on the wind tunnel measurements has been indicated through error bars superimposed to the wind tunnel measurement mean values. The elsA results correlate well with the wind tunnel measurements, lying inside the error bars or very close to them.

Figure 21 shows the comparison between the elsA results and the wind tunnel measurements in terms of the pitching moment versus incidence angle, whereas Figure 22 shows the same comparison in terms of the yawing moment versus sideslip angle. Also for the moment figures, which are normally more difficult to predict than the global forces, the engine cowling contribution, as predicted by the elsA code, compare very well with the wind tunnel measurements.

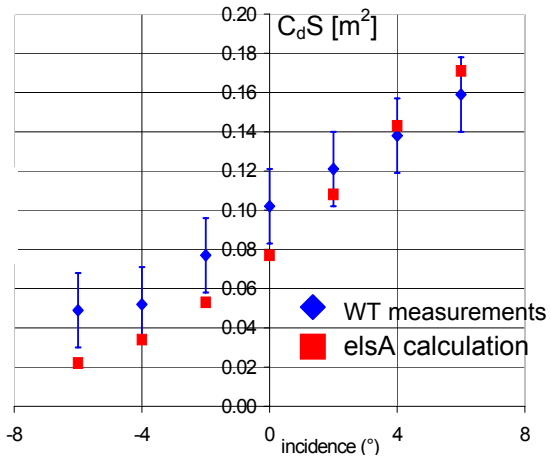

Figure 20: Contribution of the engine cowling of the NH90 model scale to the drag versus incidence angle.

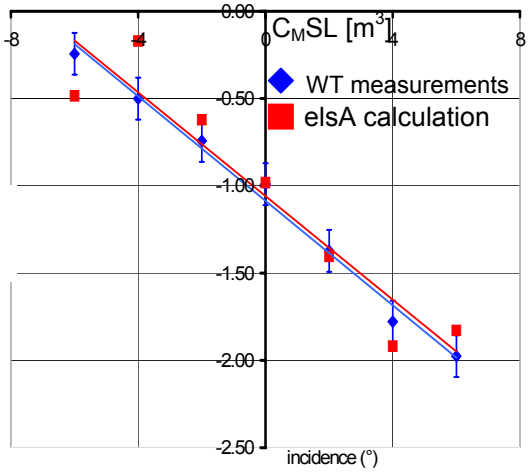

Figure 21: Contribution of the engine cowling of the NH90 model on the pitching moment versus incidence angle.

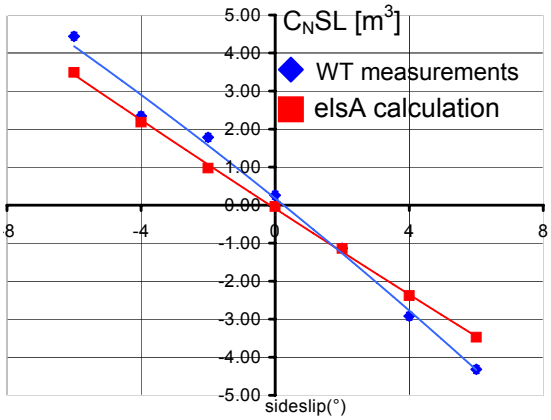

Figure 22: Contribution of the engine cowling of the NH90 model to the yawing moment versus sideslip angle.

Conclusions & Outlook

The paper presented the validation of the multi-block structured RANS flow solvers FLOWer and elsA and the unstructured RANS flow solver TAU on isolated fuselage test cases. The isolated EC145 helicopter fuselage was chosen to validate the codes FLOWer and TAU developed by DLR. The challenge related to this test case is to demonstrate the capability of the CFD tools to predict the large separation region on the backdoor of the fuselage correctly. Two different turbulence models have been used for both FLOWer (k-ω SST and RSM) and TAU (k-ω Wilcox and k-ω SST) computations. All numerical results show an excellent agreement among themselves and a fairly good agreement with the wind tunnel measurements used for this validation. The uncertainties related to the wind tunnel data and the lack of local meas-

urements, such as pressure on the surface or velocity in the field, pushed EUROCOPTER to plan a new wind tunnel campaign on the BK117-C2 model. During this wind tunnel campaign the model will be instrumented with 83 pressure ports, PIV measurements will be carried out and the laminar-turbulent transition and the separation regions will be visualised.
The elsA software developed by ONERA was validated against wind tunnel data available at EUROCOPTER. The validation test case is the NH90 model measured in the LST wind tunnel of DNW. The contribution of the engine cowling to the drag and to the pitch and yaw moments has been computed by elsA and compared with the wind tunnel measurements. These calculations show the ability of the elsA code to predict drag and moment for complex 3D helicopter fuselage shape.

Acknowledgements

The authors would like to thank the German Ministry of Economics and Labour (BMWA) and the French DPAC and DGA for their support in the framework of the CHANCE project.

References

[1] Costes, M., Pahlke, K., D'Alascio, A., Castellin, C., Altmikus, A. "*Overview of results obtained during the 6-year French-German CHANCE project*", Presented at the American Helicopter Society 61st Annual Forum, Grapevine, TX, June 13, 2005

[2] Pahlke, K., Costes, M., D'Alascio, A., Castellin, C., Altmikus, A. "The *6-year French-German CHANCE project*", 31st European Rotorcraft Forum, Florence, Italy, 13-15 September 2005

[3] Sidès, J., Pahlke, K., Costes, M., "*Numerical simulation of flows around helicopters at DLR and ONERA*", Aerospace Science and Technology, Vol. 5, pp 35-53, 2001.

[4] Kroll, N., Rossow, C.-C., Becker, K. and Thiele, F., "*The MEGAFLOW Project*" Aerospace Sciences Technology Vol. 4 (2000), pages 223-237.

[5] Kroll, N., Eisfeld, B. and Bleecke, H.M., "*The Navier-Stokes Code FLOWer*", volume 71 of Notes on Numerical Fluid Mechanics, pages 58-71. Vieweg, Braunschweig, 1999.

[6] Kroll, N., Rossow, C.C., Becker, K. and Thiele, F.: "*MEGAFLOW - A Numerical Flow Simulation System*", 21st ICAS Congress, Melbourne, paper 98-2-7.3,1998.

[7] Gerhold, T., Friedrich, O., Evans, J. and Galle, M., "*Calculation of Complex Three-Dimensional Configurations Employing the DLR TAU-Code*", AIAA Paper 97-0167, 1997.

[8] Eisfeld, B., "*Numerische Simulation aerodynamischer Probleme mit Reynolds-Spannungsmodellen*", to appear in Notes on Numerical Fluid Mechanids and Multidisciplinary Design, Springer Verlag, 2005.

[9] Eisfeld, B. and Brodersen, O., "*Advanced Tubulence Modelling and Stress Analysis for the DLR-F6 Configuration*", AIAA paper 2005-4727

[10] D'Alascio, A., Pahlke, K. and Le Chuiton, F. "*Application of a structured and an unstructured CFD-method to the fuselage aerodynamics of the EC145 helicopter. Prediction of the time averaged influence of the main rotor." European Congress on Computational Methods in Applied Sciences and Engineering, ECCOMAS 2004, Jyväskylä, 24-28 July.*

[11] ANSYS ICEMCFD, Hexa Version 5.1 User Manual, 2005

[12] CENTAUR™ 2005, www.centaursoft.com.